Rotational, Vibrational, and Electronic Modulations in N_2^+ Lasing at 391 nm: Evidence of Coherent $B^2\Sigma_u^+ - X^2\Sigma_g^+ - A^2\Pi_u$ Coupling

Toshiaki Ando,[1] Erik Lötstedt,[1] Atsushi Iwasaki,[1] Helong Li,[2] Yao Fu,[2] Siqi Wang,[2] Huailiang Xu,[2,3,*] and Kaoru Yamanouchi[1,†]

[1]Department of Chemistry, School of Science, The University of Tokyo, 7-3-1 Hongo, Bunkyo-ku, Tokyo 113-0033, Japan
[2]State Key Laboratory of Integrated Optoelectronics, College of Electronic Science and Engineering, Jilin University, Changchun 130012, China
[3]State Key Laboratory of Precision Spectroscopy, East China Normal University, Shanghai 200062, China

(Received 13 May 2019; revised manuscript received 23 August 2019; published 11 November 2019)

We investigate lasing of a N_2 gas induced by intense few-cycle near-IR laser pulses. By the pump-probe measurements, we reveal that the intensity of the $B^2\Sigma_u^+ - X^2\Sigma_g^+$ lasing emission of N_2^+ oscillates at high (0.3–0.5 PHz), medium (50–75 THz), and low (~3 THz) frequencies, corresponding to the energy separations between the rovibrational levels of the $A^2\Pi_u$ and $X^2\Sigma_g^+$ states. By solving the time-dependent Schrödinger equation, we reproduce the oscillations in the three different frequency ranges and show that the coherent population transfer among the three electronic states of N_2^+ creates the population inversion between the $B^2\Sigma_u^+$ and $X^2\Sigma_g^+$ states, resulting in the lasing at 391 nm.

DOI: 10.1103/PhysRevLett.123.203201

Interaction of molecules with an intense laser field can induce a variety of characteristic phenomena such as tunnel ionization, high-harmonic generation, and THz radiation [1–3]. In recent years, it has been revealed that nitrogen molecules (N_2), the most abundant constituent in air, and their cations (N_2^+) can be population inverted by the irradiation of intense femtosecond near-IR laser pulses. Additionally, N_2 and N_2^+ can act as gain media for cavity-free lasing in air [4–26], called "air lasing", which is of particular interest for standoff spectroscopy [4] and sensing [5–10], as well as for the macroscopic mechanism of the emission process, which was recently interpreted by superradiance [11,23].

Among the several emission bands appearing in the spectrum of air lasing, the emission at 391 nm, corresponding to the $B^2\Sigma_u^+(v'=0) - X^2\Sigma_g^+(v''=0)$ transition, has been the most attractive research subject in recent years. Because the $X^2\Sigma_g^+(v''=0)$ state is expected to be the most populated state when N_2^+ emerges after the tunneling ionization of N_2, the mechanism of the population transfer from the $X^2\Sigma_g^+(v''=0)$ state to the $B^2\Sigma_u^+(v'=0)$ state, so that the population inversion is achieved, has been mysterious for many years. Furthermore, a variety of scenarios such as rotational excitation [11,12] and multiple-state optical coupling [13,14] have been proposed as postionization processes.

In Ref. [13], we showed that the population inversion between the $B^2\Sigma_u^+$ and $X^2\Sigma_g^+$ states of N_2^+ can be achieved using sub-10-fs laser pulses through the electronic transitions occurring immediately after N_2^+ is created within the laser pulse. We also showed experimentally that the intensity of the lasing emission is enhanced by 2 orders of magnitude by modulating the polarization state of the laser pulses [15], indicating that the population transfer from the $X^2\Sigma_g^+$ state to the $A^2\Pi_u$ state enhances the population inversion between the $B^2\Sigma_u^+(v'=0)$ and $X^2\Sigma_g^+(v''=0)$ states.

Our recent theoretical studies [27,28] based on Floquet modeling also supported the experimental interpretations. The scenario we proposed can be referred to as the postionization three-state ($B^2\Sigma_u^+$, $A^2\Pi_u$, and $X^2\Sigma_g^+$) coupling model and can be interpreted as follows: (i) N_2^+ preferentially formed at the maximum of the electric field amplitude is suddenly exposed to the intense near-IR laser field, and this sudden turn-on of the laser electric field induces a nonresonant population transfer from the $X^2\Sigma_g^+$ state to the $B^2\Sigma_u^+$ state of N_2^+ [27]. (ii) The population in the $X^2\Sigma_g^+$ state is depleted further through the $A^2\Pi_u$–$X^2\Sigma_g^+$ transition induced resonantly by the later part of the intense near-IR laser field [28]. Indeed, it was reported recently by pump-probe measurements using near-IR laser pulses that the $A^2\Pi_u$ $(v'=2)$ state and the $X^2\Sigma_g^+(v''=0)$ state are coherently coupled [26]. Even though the two-step scenario above explains the air lasing at 391 nm, it has not been certain how much the $A^2\Pi_u$–$X^2\Sigma_g^+$ coupling could enhance the air lasing at 391 nm or how the respective $A^2\Pi_u$–$X^2\Sigma_g^+$ (v', v'') transitions contribute to the enhancement.

In the present Letter, in order to clarify the role of the $A^2\Pi_u$–$X^2\Sigma_g^+$ transition in the population inversion between the $B^2\Sigma_u^+$ and $X^2\Sigma_g^+$ states of N_2^+, we perform pump-probe measurements of the lasing emission at 391 nm using

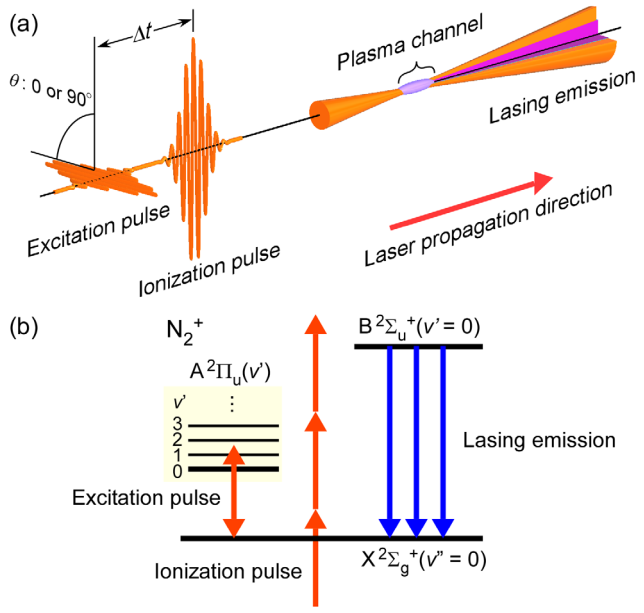

FIG. 1. (a) Schematic diagram for the ionization and excitation experiment. (b) Energy diagram for the enhancement of the lasing signal of $B^2\Sigma_u^+(v'=0)$–$X^2\Sigma_g^+(v''=0)$ through the three-state coupling scheme.

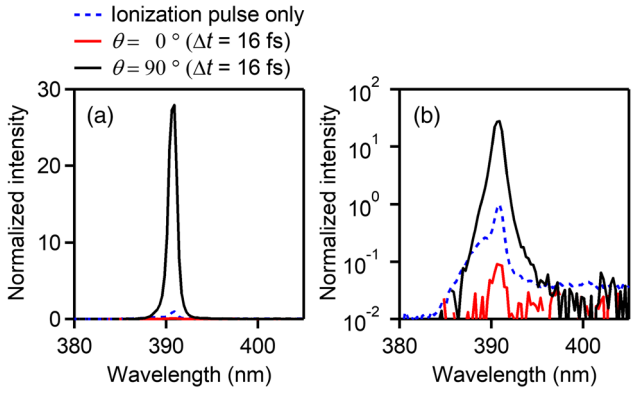

FIG. 2. Forward spectra in a (a) linear scale and (b) logarithmic scale: the spectra obtained with the ionization pulses only (blue dotted curve) and those obtained at $\theta = 0°$ (red curve) and $\theta = 90°$ (black curve) with the ionization and excitation pulses. The lasing intensity is normalized by the lasing intensity at 391 nm recorded only with the ionization pulses.

few-cycle laser pulses. By the pump-probe measurements, we are able to extract the effect of the postionization process without disturbing the ionization process, and consequently, we show that the lasing intensity is modulated with the frequencies of the $A^2\Pi_u$–$X^2\Sigma_g^+$ rovibronic transitions occurring after the creation of population inverted N_2^+, in which the rotational and vibrational states of all the three electronic states are involved.

As shown in Fig. 1, we first create the population inversion in N_2^+ by introducing an intense laser pulse (an ionization pulse: ~7 fs, 800 nm, 40 μJ/pulse) whose ellipticity is 0.1. After a certain time delay Δt, we introduce a weaker laser pulse (an excitation pulse: ~7 fs, 800 nm, 20 μJ/pulse), whose polarization direction with respect to that of the pump pulse is set to be θ, to induce the $A^2\Pi_u$–$X^2\Sigma_g^+$ (v', v'') transitions ($v' = 1$, 2, and 3, and $v'' = 0$). By monitoring the $B^2\Sigma_u^+$–$X^2\Sigma_g^+$ lasing intensity as a function of the pump-probe time delay, we investigate how the $A^2\Pi_u$–$X^2\Sigma_g^+$ coupling contributes to the population inversion between the $B^2\Sigma_u^+$ and $X^2\Sigma_g^+$ states (see Supplemental Material for the experimental details [29]).

Figure 2 shows the spectra of the forwardly propagating light in the wavelength range of 380–410 nm. The peak at 391 nm corresponds to the lasing emission of the $B^2\Sigma_u^+$ $(v'=0) - X^2\Sigma_g^+$ $(v''=0)$ transition of N_2^+. As shown in Fig. 2, because the lasing signal (in blue) appeared using the ionization pulse only, it is confirmed that the population inversion between $B^2\Sigma_u^+$ $(v'=0)$ and $X^2\Sigma_g^+$ $(v''=0)$ can be achieved using the ionization pulse only.

When the excitation pulse was introduced 16 fs after the ionization pulse with the perpendicular polarization configuration ($\theta = 90°$), the lasing intensity was ~30 times stronger than that obtained only by using the ionization pulse. We consider that this enhancement of the lasing signal was achieved because the population in the $X^2\Sigma_g^+$ state is efficiently transferred to the $A^2\Pi_u$ state through the $A^2\Pi_u$–$X^2\Sigma_g^+$ transition induced by the excitation pulse in a similar scheme proposed in our previous Letter [15].

On the other hand, when the polarization of the excitation pulse is parallel ($\theta = 0°$) with respect to the ionization pulse, the intensity of the lasing signal becomes one order of magnitude smaller than that obtained only by using the ionization pulse. This decrease in the lasing intensity can be ascribed to the fact that the population in $X^2\Sigma_g^+$ $(v''=0)$ in the ensemble of N_2^+ increases by the excitation pulse, whose intensity is so weak that only the population in $X^2\Sigma_g^+$ $(v''=0)$ is increased through the ionization of neutral N_2 remaining in the gas sample, resulting in the decrease in the $B^2\Sigma_u^+$–$X^2\Sigma_g^+$ lasing intensity. On the basis of the results of the theoretical calculations presented in Ref. [36], the amount of N_2^+ created by the excitation pulse is estimated to be about 10% of that created by the ionization pulse [36], which is consistent with the observation that the lasing intensity becomes smaller by one order of magnitude.

In order to examine the effect of the $A^2\Pi_u$–$X^2\Sigma_g^+$ transition induced by the excitation pulse, the lasing intensity at 391 nm is plotted as a function of Δt as shown in Fig. 3 for the two cases of $\theta = 0°$ (red curve) and $\theta = 90°$ (black curve). When $\theta = 0°$, the lasing intensity becomes minimum at ~35 fs and maximum at ~200 fs. On the contrary, when $\theta = 90°$, the lasing intensity becomes maximum at ~15 fs and minimum at ~200 fs. These slow modulations in the lasing intensities with the frequency

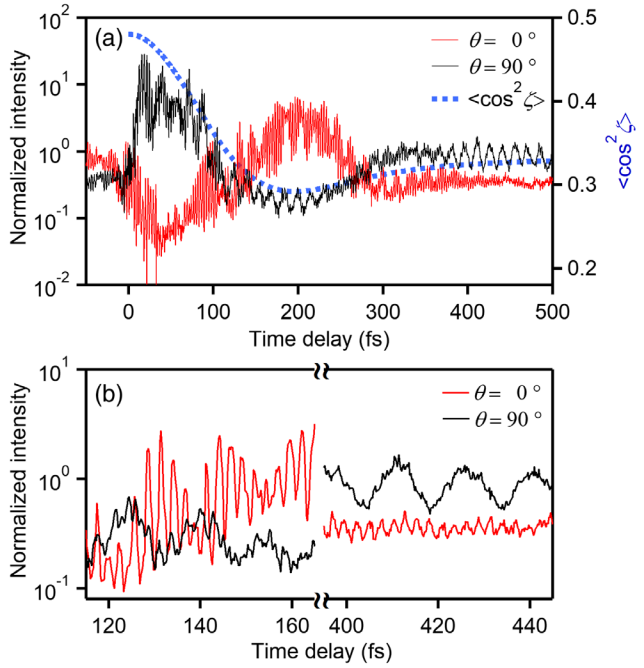

FIG. 3. (a) The time-dependent lasing intensities of N_2^+ at 391 nm when $\theta = 0°$ (red curve) and $\theta = 90°$ (black curve) and the expectation value of $\cos^2\zeta$ at $T = 295$ K (blue dotted curve). The rotational wave packet is assumed to be created by the ζ–dependent tunneling ionization [34] and $B = 1.931\,76$ cm^{-1} is adopted as the rotational constant of N_2^+ [35] (see Supplemental Material [29]). (b) Expanded view of the lasing intensity when $\theta = 0°$ (red curve) and $\theta = 90°$ (black curve) in the ranges of 115–165 and 395–445 fs.

of ~3 THz exhibiting the antiphase behaviors can be ascribed to the rotational motion of N_2^+.

In Fig. 3(a), with the dotted line, the field-free time evolution of the expectation value of $\cos^2\zeta$, $\langle\cos^2\zeta\rangle(t)$, derived from the theoretical calculations described in the Supplemental Material, is plotted with the dotted line [29], where ζ denotes the angle between the N-N molecular axis and the polarization vector of the ionization laser pulse. The $\langle\cos^2\zeta\rangle(t)$ value decreases from $\langle\cos^2\zeta\rangle = 0.48$ at $t = 0$ to the minimum value of $\langle\cos^2\zeta\rangle = 0.29$ at $t = 195$ fs. When $\theta = 90°$, the variation of the lasing intensity is in phase with $\langle\cos^2\zeta\rangle(t)$, while, when $\theta = 0°$, the variation of the lasing intensity is in antiphase with $\langle\cos^2\zeta\rangle(t)$. This means that the lasing intensity is enhanced when the polarization direction of the excitation pulse is perpendicular to the N-N molecular axis, and consequently, the intensity of the $B^2\Sigma_u^+$ $(v' = 0)$–$X^2\Sigma_g^+$ $(v'' = 0)$ lasing of N_2^+ is enhanced by the perpendicular $A^2\Pi_u$–$X^2\Sigma_g^+$ transition.

It can also be seen in Fig. 3(a), and more clearly in Fig. 3(b), which is the expanded view of Fig. 3(a) in the time ranges of 115–165 and 395–445 fs, the lasing intensities oscillate at two different frequencies, i.e., the higher frequency (0.3–0.5 PHz) component (corresponding to the period of 2–3 fs) and the lower frequency (50–75 THz) component (corresponding to the period of 13–20 fs). The higher frequency component corresponds to the energy separations between the rovibrational levels in the $A^2\Sigma_u^+$ state and those in the $X^2\Sigma_g^+$ state of N_2^+. The lower frequency component is composed of the vibrational level separations within the three respective electronic states of $B^2\Sigma_u^+$, $A^2\Pi_u$, and $X^2\Sigma_g^+$, which shows that the vibronic levels in the three electronic states are coupled coherently, resulting in the modulation in the $B^2\Sigma_u^+$–$X^2\Sigma_g^+$ lasing. Recently, the oscillation at 0.38 PHz, corresponding to the energy separation between the $v' = 2$ state in the $A^2\Pi_u$ state and the $v'' = 0$ state in the $X^2\Sigma_g^+$ state, was also identified [26].

As shown in Fig. 3(b), the high-frequency oscillations can also be seen in the delayed time range of 115–165 fs in the case of $\theta = 90°$, even though the amplitude is only one-tenth of that in the case of $\theta = 0°$. This higher frequency oscillation, which should not appear if the polarization direction of the pump and probe laser pulses are exactly perpendicular, is ascribed to the small ellipticity (~0.1) of the few-cycle laser pulses.

In order to identify securely the origins of the frequency components at 0.3–0.5 PHz and 50–75 THz, the lasing signals are Fourier transformed. Figure 4(a) shows the Fourier transform of the lasing intensity $A(\omega)$, defined as

$$A(\omega) = \left| \int W(t) \ln[S(t)] \exp(i\omega t) dt \right|, \qquad (1)$$

where $S(t)$ is the lasing intensity at 391 nm and $W(t)$ is a window function, $W(t) = \exp\{-[(t - 320\text{ fs})/140\text{ fs}]^4\}$, which is introduced to remove the optical interference between the ionization and excitation laser pulses. Because the lasing signal is considered to be proportional to the exponential of the population difference between the $B^2\Sigma_u^+(v' = 0)$ state and the $X^2\Sigma_g^+(v'' = 0)$ state, the Fourier transform is performed using the logarithm of the lasing intensities. When $\theta = 0°$, three peaks appear at 0.33, 0.38, and 0.44 PHz in Fig. 4(a), and, when $\theta = 90°$, two peaks appear at 0.33 and 0.38 PHz with the relatively weak amplitudes. These peaks are assigned to the transition between the vibrational levels ($v' = 1$, 2, and 3) of the $A^2\Pi_u$ state and the vibrational level ($v'' = 0$) of the $X^2\Sigma_g^+$ state, which shows that the $A^2\Pi_u$–$X^2\Sigma_g^+$ transitions induced by the excitation pulse enhance the lasing intensity. The peaks at 54, 66, and 72 THz are assigned, respectively, to the vibrational energy separations within the $A^2\Pi_u$, $X^2\Sigma_g^+$, and $B^2\Sigma_u^+$ states of N_2^+.

In order to confirm the interpretation of the rapid oscillations in the lasing signal described above, we simulated numerically the time-dependent population dynamics in the $X^2\Sigma_g^+$, $A^2\Pi_u$, and $B^2\Sigma_u^+$ states of N_2^+ by adopting the three-state coupling model, as proposed by us in [13], and performed the Fourier transform of the population difference between the $B^2\Sigma_u^+(v' = 0)$ state and the $X^2\Sigma_g^+(v'' = 0)$ state

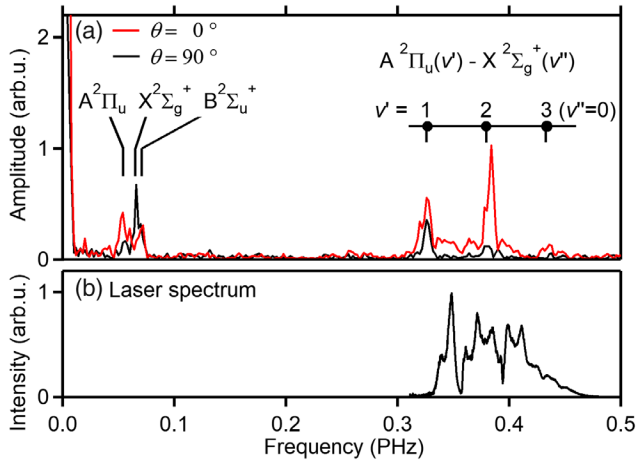

FIG. 4. (a) Fourier transform spectra of the lasing intensity at 391 nm recorded when $\theta = 0°$ (red curve) and $\theta = 90°$ (black curve) with the vibrational and electronic state assignment. It is possible that the vibrational frequency (70 THz) of the $X^1\Sigma_g^+$ state of N_2 contributes to the peak at 72 THz because the ionization pulse can also excite coherently the vibration of N_2 and the probability of the ionization by the excitation pulse oscillates with the vibrational period of N_2. (b) Spectrum of the few-cycle near-IR laser pulses whose frequency range covers the $A^2\Pi_u$ ($v' = 1$, 2, and 3)–$X^2\Sigma_g^+(v'' = 0)$ transitions.

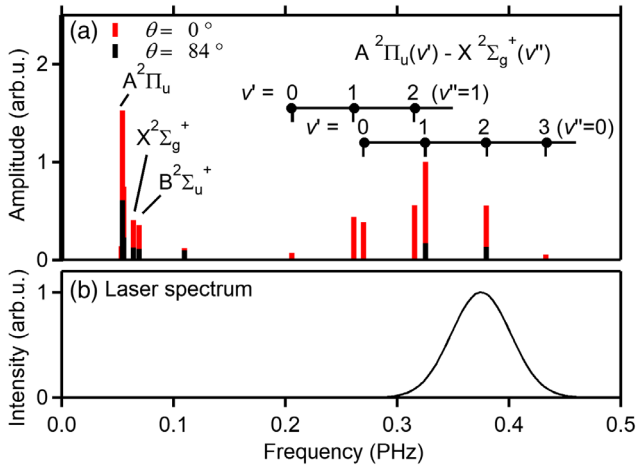

FIG. 5. (a) The normalized Fourier transforms of the population difference between the $B^2\Sigma_u^+(v' = 0)$ state and the $X^2\Sigma_g^+(v'' = 0)$ state calculated at $\theta = 0°$ and $\theta = 84°$. Only the peak profiles whose amplitudes are larger than 0.05 are shown. The vibrational assignments of the $A^2\Pi_u(v')$ and $X^2\Sigma_g^+(v'')$ states are also shown. In the low-frequency region below 0.12 PHz, the vibrational energy separations within the respective three electronic states ($B^2\Sigma_u^+$, $A^2\Pi_u$, and $X^2\Sigma_g^+$) of N_2^+ appear. (b) The spectrum of the excitation laser pulse ($\lambda = 800$ nm, 7 fs FWHM) adopted in the numerical simulation.

(see Supplemental Material for details in the numerical calculations [29]).

In Fig. 5(a), the Fourier transform spectra obtained using the laser parameters [$\lambda = 800$ nm, $\tau = 7$ fs (FWHM), $I_{\text{ionization}}=4\times10^{14}\text{W/cm}^2$, and $I_{\text{excitation}}=2\times10^{14}\text{W/cm}^2$], which are close to the experimental ones, are shown for the two polarization angles $\theta = 0°$ and $\theta = 84°$. The polarization angle $\theta = 84°$ is chosen so that $|\boldsymbol{E}_{\text{ion}} \cdot \boldsymbol{E}_{\text{excit}}|/|\boldsymbol{E}_{\text{ion}}||\boldsymbol{E}_{\text{excit}}| = 0.1$, corresponding to the ellipticity of the laser pulses in the experiment.

As shown in Fig. 5(a), the Fourier amplitudes exhibiting the pronounced peaks at the frequencies of the $A^2\Pi_u$–$X^2\Sigma_g^+$ $(v', v'') = (1, 0)$ and (2,0) transitions, as well as the vibrational energy separations of the three electronic states, are in good agreement with the experimental spectra shown in Fig. 4(a). In the theoretical spectrum, the peaks of $(v', v'') = (0, 0)$, (1, 1), and (2, 1), which are not identified in Fig. 4(a), appear and the (1, 0) peak is relatively smaller than that in the experimental spectra. These discrepancies can be ascribed to the fact that the tail part of the spectral band of the theoretical excitation laser pulse stretches toward the lower frequency region than the excitation pulse in the experiment. When the polarization direction of the ionization pulse and that of the excitation pulse are almost perpendicular to each other ($\theta = 84°$), the amplitudes of the peaks in Fig. 5(a) become smaller than those at $\theta = 0°$, which is consistent with the experimental results.

In summary, we have irradiated a N_2 gas with a pair of linearly polarized intense near-IR few-cycle laser pulses, i.e., the ionization laser pulse and the excitation laser pulse, to generate coherent lasing of the $B^2\Sigma_u^+$–$X^2\Sigma_g^+$ transition at 391 nm. When the delay time is 16 fs, the lasing intensity achieved when $\theta = 90°$ is about 300 times larger than that achieved when $\theta = 0°$, showing that the perpendicular $A^2\Pi_u$–$X^2\Sigma_g^+$ transition efficiently depletes the $X^2\Sigma_g^+$ state population. By varying the time delay between these two pulses, we have found that the $B^2\Sigma_u^+$–$X^2\Sigma_g^+$ lasing intensity is modulated with the high (0.3–0.5 PHz), medium (50–75 THz), and low (~3 THz) frequencies and have identified by the Fourier analysis that these frequencies represent the energy separations between the rovibrational levels of the $B^2\Sigma_u^+$, $A^2\Pi_u$, and $X^2\Sigma_g^+$ states, corresponding to the electronic, vibrational, and rotational modulations, respectively. By the numerical simulation based on the postionization three-state coupling model, we have reproduced these three kinds of modulations covering the PHz–THz frequency region quantitatively. Supported by the unambiguous spectroscopic assignments of the Fourier transformed data, our experimental and theoretical results have shown decisively that the three electronic states, $B^2\Sigma_u^+$, $A^2\Pi_u$, and $X^2\Sigma_g^+$, are coherently coupled in the N_2^+ lasing at 391 nm. The present approach in which the time domain pump-probe data are Fourier transformed has general applicability to the characterization of lasing phenomena of atoms and molecules induced by ultrashort laser pulses.

This work is supported in part by National Natural Science Foundation of China (NSFC) (61625501,

61427816) and by the MEXT (Ministry of Education, Culture, Sports, Science and Technology) Grant-in-Aid for Specially Promoted Research (No. 15H05696).

*huailiang@jlu.edu.cn
†kaoru@chem.s.u-tokyo.ac.jp

[1] L. V. Keldysh, Sov. Phys. JETP **20**, 1307 (1965).
[2] M. Ferray, A. L'Huillier, X. F. Li, L. A. Lompre, G. Mainfray, and C. Manus, J. Phys. B **21**, L31 (1988).
[3] J. Liu, J. Dai, S. L. Chin, and X.-C. Zhang, Nat. Photonics **4**, 627 (2010).
[4] P. R. Hemmer, R. B. Miles, P. Polynkin, T. Siebert, A. V. Sokolov, P. Sprangle, and M. O. Scully, Proc. Natl. Acad. Sci. U.S.A. **108**, 3130 (2011).
[5] Q. Luo, W. Liu, and S. L. Chin, Appl. Phys. B **76**, 337 (2003).
[6] J. Yao, B. Zeng, H. Xu, G. Li, W. Chu, J. Ni, H. Zhang, S. L. Chin, Y. Cheng, and Z. Xu, Phys. Rev. A **84**, 051802(R) (2011).
[7] D. Kartashov, S. Ališauskas, A. Baltuška, A. Schmitt-Sody, W. Roach, and P. Polynkin, Phys. Rev. A **88**, 041805(R) (2013).
[8] T.-J. Wang, J. Ju, J.-F. Daigle, S. Yuan, R. Li, and S. L. Chin, Laser Phys. Lett. **10**, 125401 (2013).
[9] J. Ni, W. Chu, H. Zhang, B. Zeng, J. Yao, L. Qiao, G. Li, C. Jing, H. Xie, H. Xu, Y. Cheng, and Z. Xu, Opt. Lett. **39**, 2250 (2014).
[10] P. Ding, S. Mitryukovskiy, A. Houard, E. Oliva, A. Couairon, A. Mysyrowicz, and Y. Liu, Opt. Express **22**, 29964 (2014).
[11] A. Azarm, P. Corkum, and P. Polynkin, Phys. Rev. A **96**, 051401(R) (2017).
[12] M. Lei, C. Wu, A. Zhang, Q. Gong, and H. Jiang, Opt. Express **25**, 4535 (2017).
[13] H. Xu, E. Lötstedt, A. Iwasaki, and K. Yamanouchi, Nat. Commun. **6**, 8347 (2015).
[14] J. Yao, S. Jiang, W. Chu, B. Zeng, C. Wu, R. Lu, Z. Li, H. Xie, G. Li, C. Yu, Z. Wang, H. Jiang, Q. Gong, and Y. Cheng, Phys. Rev. Lett. **116**, 143007 (2016).
[15] H. Li, M. Hou, H. Zang, Y. Fu, E. Lötstedt, T. Ando, A. Iwasaki, K. Yamanouchi, and H. Xu, Phys. Rev. Lett. **122**, 013202 (2019).
[16] M. Britton, P. Laferrière, D. H. Ko, Z. Li, F. Kong, G. Brown, A. Naumov, C. Zhang, L. Arissian, and P. B. Corkum, Phys. Rev. Lett. **120**, 133208 (2018).
[17] P. Ding, E. Oliva, A. Houard, A. Mysyrowicz, and Y. Liu, Phys. Rev. A **94**, 043824 (2016).
[18] H. Zhang, C. Jing, J. Yao, G. Li, B. Zeng, W. Chu, J. Ni, H. Xie, H. Xu, S. L. Chin, K. Yamanouchi, Y. Cheng, and Z. Xu, Phys. Rev. X **3**, 041009 (2013).
[19] S. Mitryukovskiy, Y. Liu, P. Ding, A. Houard, and A. Mysyrowicz, Opt. Express **22**, 12750 (2014).
[20] G. Point, Y. Liu, Y. Brelet, S. Mitryukovskiy, P. Ding, A. Houard, and A. Mysyrowicz, Opt. Lett. **39**, 1725 (2014).
[21] J. Yao, H. Xie, B. Zeng, W. Chu, G. Li, J. Ni, H. Zhang, C. Jing, C. Zhang, H. Xu, Y. Cheng, and Z. Xu, Opt. Express **22**, 19005 (2014).
[22] H. Xu, E. Lötstedt, T. Ando, A. Iwasaki, and K. Yamanouchi, Phys. Rev. A **96**, 041401(R) (2017).
[23] A. Zhang, Q. Liang, M. Lei, L. Yuan, Y. Liu, Z. Fan, X. Zhang, S. Zhuang, C. Wu, Q. Gong, and H. Jiang, Opt. Express **27**, 12638 (2019).
[24] M. Clerici, A. Bruhács, D. Faccio, M. Peccianti, M. Spanner, A. Markov, B. E. Schmidt, T. Ozaki, F. Légaré, F. Vidal, and R. Morandotti, Phys. Rev. A **99**, 053802 (2019).
[25] Y. Liu, P. Ding, G. Lambert, A. Houard, V. Tikhonchuk, and A. Mysyrowicz, Phys. Rev. Lett. **115**, 133203 (2015).
[26] A. Zhang, M. Lei, J. Gao, C. Wu, Q. Gong, and H. Jiang, Opt. Express **27**, 14922 (2019).
[27] Y. Zhang, E. Lötstedt, and K. Yamanouchi, J. Phys. B **50**, 185603 (2017).
[28] Y. Zhang, E. Lötstedt, and K. Yamanouchi, J. Phys. B **52**, 055401 (2019).
[29] See Supplemental Material at http://link.aps.org/supplemental/10.1103/PhysRevLett.123.203201 for details of the experiments and theoretical calculations, which includes Refs. [22,30–35].
[30] J. R. Birge, R. Ell, and F. X. Kärtner, Opt. Lett. **31**, 2063 (2006).
[31] H. Stapelfeldt and T. Seideman, Rev. Mod. Phys. **75**, 543 (2003).
[32] S. R. Langhoff, C. W. Bauschlicher, and H. Partridge, J. Chem. Phys. **87**, 4716 (1987).
[33] S. R. Langhoff and C. W. Bauschlicher, J. Chem. Phys. **88**, 329 (1988).
[34] S.-F. Zhao, C. Jin, A.-T. Le, T. F. Jiang, and C. D. Lin, Phys. Rev. A **81**, 033423 (2010).
[35] E. A. Colbourn and A. E. Douglas, J. Mol. Spectrosc. **65**, 332 (1977).
[36] M. Spanner and S. Patchkovskii, Chem. Phys. **414**, 10 (2013).